Chemical Engineering Journal 424 (2021) 130524

Contents lists available at ScienceDirect

Chemical Engineering Journal

journal homepage: www.elsevier.com/locate/cej

Stabilization effect of solid-electrolyte interphase by electrolyte engineering for advanced Li-ion batteries

His Muhammad Bintang [a,b], Seongsoo Lee [a,c], Sunghee Shin [a], Byung Gon Kim [d], Hun-Gi Jung [a,b], Dongmok Whang [c], Hee-Dae Lim [a,b,*]

[a] Center for Energy Storage Research, Korea Institute of Science and Technology (KIST), Seoul 02792, South Korea
[b] Division of Energy & Environment Technology, KIST School, Korea University of Science and Technology (UST), Seoul 02792, South Korea
[c] SKKU Advanced Institute of Nanotechnology (SAINT) and School of Advanced Materials Science and Engineering, Sungkyunkwan University, Suwon 16419, South Korea
[d] Next Generation Battery Research Center, Korea Electrotechnology Research Institute (KERI), Changwon-si 51543, South Korea

ARTICLE INFO

Keywords:
Succinonitrile
Sn anode
Solid electrolyte interphase
Inorganic SEI layer

ABSTRACT

Sn-based materials have been highlighted as promising anodes for next-generation batteries; however, such alloying-based anodes suffer from gradual cell degradation caused by the associated large volume changes, leading to particle pulverization and an unstable solid electrolyte interphase (SEI). A key to constructing a stable SEI as well as effectively buffering the large volume expansion is to establish appropriate electrolyte conditions. In this work, to induce the formation of a favorable SEI layer, a Sn anode is paired with an electrolyte composed of eutectic succinonitrile (SN) combined with fluoroethylene carbonate (FEC) for the first time. Whereas conventional electrolytes are prone to form organic SEI components, which are vulnerable to large volume changes, the combination of SN and FEC enables the formation of a mechanically rigid SEI that is mainly composed of favorable inorganics such as LiF and Li_3N. The synergistic effects of SN and FEC result in superior cycle performance of the Sn anode with improved efficiency compared with that achieved using conventional carbonate electrolytes. The modified SEI layer was closely investigated using various surface analysis techniques, with the individual effects of SN and FEC extracted. The rational design of the electrolyte provides a simple yet effective approach to enhance the electrochemical performance of Sn anodes and can be further extended to other alloying-based anode materials.

1. Introduction

The rapidly growing markets of large electrical devices, representatively electric vehicles (EVs), have naturally led to increased interest in developing the development of next-generation batteries. Among many candidates, alloying materials (*e.g.*, Si, Ge, Sn, Pb, *etc.*) have been considered as promising substitutes for the conventional graphite anode owing to their high energy densities [1–3]. The limited capacity of the intercalation-based graphite host makes it difficult to meet the rapidly increasing demands for high-performance Li-ion batteries (LIBs) and to sufficiently power next-generation large-scale devices. In contrast, alloying materials show great potential to deliver exceptional energy-storage capability far beyond that of graphite [3,4]. Among the many alloying anodes, Sn has attracted particular attention because of its unique advantages. Sn has a high theoretical volumetric capacity of 2,562 Ah L^{-1} ($Li_{4.4}Sn$), which is much higher than that of graphite (804 Ah L^{-1}) and even Li metal (2,062 Ah L^{-1}) [4]. In addition, the relatively small volume expansion of a Sn anode (259%) compared with that of a Si anode (420%) is highly advantageous in terms of practical applications. Moreover, Sn is a reasonably inexpensive material owing to the abundance of resources in nature and has lower toxicity than other alloying materials [3–5].

However, despite the relatively small volume changes of Sn compared with those of other alloying materials, it still suffers from cell degradation associated with its volume expansion. Throughout electrochemical cycles, Sn particles are vulnerable to cracking and pulverization, causing the electrical isolation of the active material from the current collector. Moreover, the pulverized particles simultaneously contribute to the more serious problem of an unstable solid electrolyte interphase (SEI) [6,7]. The repeated volume changes known as the

* Corresponding author.
E-mail address: hdlim@kist.re.kr (H.-D. Lim).

https://doi.org/10.1016/j.cej.2021.130524
Received 8 March 2021; Received in revised form 12 May 2021; Accepted 23 May 2021
Available online 27 May 2021

"breathing effect"[8] provoke dynamic changes in both the thickness and composition of the SEI, resulting in unstable passivating behavior of the Sn interface. The SEI components formed in conventional liquid electrolytes (CLEs) are mainly composed of lithium ethylene dicarbonate (LEDC) from the reduction of the carbonate solvent [9,10], and this component lacks sufficient mechanical strength and ionic conductivity [11–13]. The weak LEDC and other organic-based components are prone to partially break and dissolve, leading to the unstable and porous SEI layer [10,14,15]. Thus, the conventional electrolyte systems are insufficient to effectively mitigate the breathing of pulverized particles. To protect Sn particles from the unstable SEI, various architectural designs of Sn[16,17] or coating methods have been proposed [17,18]. However, the popular approaches are relatively complex and high cost, significantly hindering their practical application.

To overcome the current hurdles facing Sn anodes, it is necessary to develop a new approach that induces the formation of a robust and dense inorganic SEI instead of one composed of organic components. The use of fluoroethylene carbonate (FEC) as the electrolyte additive to stabilize the SEI in conventional electrolyte systems has been investigated as a typical solution [19–25]. The FEC additive simply induces the formation of an inorganic SEI layer, which is more favorable than the unstable organic components [10,26,27]. However, for Sn anodes, the use of FEC may not be acceptable because preservation of the original film is difficult due to the dynamic volume changes during cycling. In addition, the application of the FEC additive for Sn anodes has been limited because the unstable organic components are likely to form prior to the formation of inorganic SEI layer [28,29]. Also, the application of the FEC additive for Sn anodes has been limited, especially for nano-sized particles (less than10 nm) and thin films [23,24], and its practical use with macro-sized Sn has not been satisfactory. The prevailing issues facing Sn anodes have inspired us to explore an alternative electrolyte system to achieve a stable SEI and improve the electrochemical performance.

In this study, we developed a new electrolyte system by combining the FEC additive with the plastic-crystal succinonitrile (SN) to simply induce the formation of a robust and stable SEI layer on Sn particles. SN in the eutectic phase shows great potential as an alternative electrolyte owing to its high polarity, thermal stability, and tunable phase properties [30–33]. SN was particularly selected to prevent the formation of the organic-rich phase (LEDC) while, at the same time, forming an inorganic-based SEI on the Sn anode. Our findings demonstrate that the combined use of SN and FEC is responsible for forming a rigid and stable SEI mainly composed of the ideal components of LiF and Li_3N. The synergistic effects of SN and FEC, attributing to the compositional change of the SEI, successfully drive the formation of a dense and stable inorganic SEI layer, resulting in improved electrochemical performance.

2. Results and discussion

To validate the use of the new electrolyte for a Sn anode, the individual effects of FEC and SN must first be identified. Therefore, different electrolytes were prepared, and their effects on the electrochemical performance were compared. The SN-based electrolyte without FEC (i.e., SNE) was prepared by dissolving 1 M LiTFSI salt in SN, and the one with FEC (SNFEC) was prepared by additionally adding 5 wt% FEC. The compositions of the prepared electrolytes were confirmed using Fourier-transform infrared spectroscopy (FT-IR), as shown in Fig. 1a. The FT-IR spectra verified that both LiTFSI and FEC were well dissolved in the SN matrix, with the appearance of the characteristic peaks of LiTFSI and FEC at around 1,200 and 1,800 cm^{-1}, respectively [34]. Differential scanning calorimetry (DSC) was also used to evaluate the phase-transition behaviors of the SN-based electrolytes after the additions of LiTFSI and FEC (Fig. 1b). The original melting point (T_{mp}) of pure SN (red line) is approximately 60 °C; however, it shifted to 17.5 °C after the addition of 1 M LiTFSI (SNE, blue line), with a similar T_{mp} maintained after the addition of FEC (SNFEC, green line). The shift of T_{mp} is an important factor. Whereas pure SN is in a quasi-solid state at room temperature (RT), the lowered T_{mp} resulting from the addition of salt enables its use in the liquid state at RT. Additionally, their phase transitions under various temperatures were investigated in **Figure S1**. This result indicates that the properties of the SNE and SNFEC electrolytes with 1 M of salt are appropriate for their use as eutectic liquid ion-conducting agents.

It is also essential to verify whether the electrolytes are chemically stable with Li metal, considering that SN was reported to be polymerized when directly facing Li metal [30]. We investigated the feasibility of their use by immersing Li metal in each electrolyte (Fig. 1c). In the absence of FEC, SNE underwent a slow side reaction with Li metal, gradually turning black due to the polymerization. In contrast, SNFEC appeared to maintain its original color even after 1 week. It should be

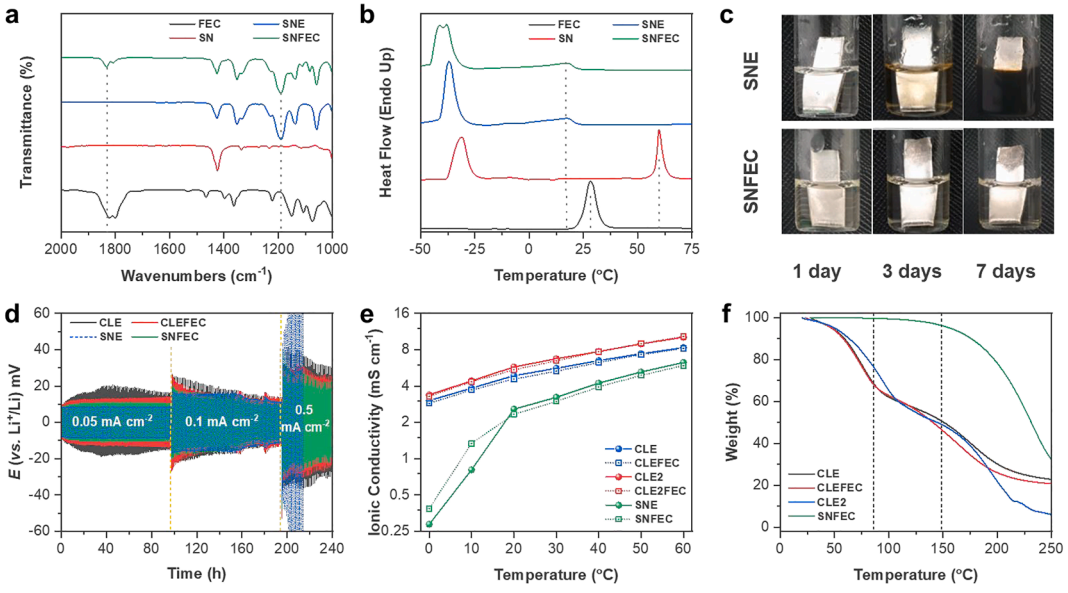

Fig. 1. Characterization of SN-based electrolytes without FEC (SNE) and with FEC (SNFEC). (a) FT-IR, (b) DSC analyses, and (c) reaction test with Li metal of prepared SNE and SNFEC electrolytes. (d) Li symmetric stripping–deposition test at various current densities at 30 °C, (e) temperature-dependent ionic conductivities, and (f) TGA results for the various electrolytes.

noted that FEC can mitigate the undesired polymerization of SN by spontaneously forming a protective layer on the Li metal surface [33,35], which is one reason why we added a sufficient amount of 5 wt% FEC in SNFEC [33,34].

To investigate the effects of SN and FEC in electrochemical cycling, a Li^+ deposition and stripping test was conducted (Fig. 1**d**). Li symmetric cells were prepared and tested at current densities of 0.05, 0.1, and 0.5 mA cm^{-2} at 30 °C for 240 h. The initial cycling with SNE at 0.05 mA cm^{-2} appeared to be stable with acceptable overpotentials; however, large polarizations were observed at the high rate of 0.5 mA cm^{-2}, leading to cell failure after ~ 8 days. As similarly observed in the reaction test (Fig. 1**c**), the polymerized SN on Li metal greatly hindered ion transfer and almost passivated the metal after 7 days. In contrast, the cells using conventional electrolytes of CLE and CLEFEC (CLE with FEC additive) showed stable Li^+ stripping–deposition behaviors. The cell with CLEFEC showed a slightly lower polarization than that using the additive-free CLE because the FEC prevented the random deposition at the surface of Li metal and suppressed the Li dendrite growth [20,33]. Notably, the cell with SNFEC showed the lowest polarizations for the entire current range from 0.05 to 0.5 mA cm^{-2}. Even for prolonged cycles, the SNFEC cell could maintain the low polarization. These results demonstrate the applicability of SNFEC in a half-cell configuration composed of Li metal as the counter electrode and Sn as the working electrode.

To compare the ionic conductivities of the electrolytes, the temperature-dependent conductivities from 0 °C to 60 °C were measured in a blocking-cell system (Fig. 1**e**). As control groups, LiTFSI (CLE) and $LiPF_6$ (CLE2) in ethylene carbonate (EC) and diethyl carbonate (DEC) (1:1 vol ratio) were also compared. Because of the low viscosity of the carbonate-based electrolytes, CLE and CLE2 exhibited high conductivities of 5.6 and 6.7 mS cm^{-1} at 30 °C, respectively, whereas SNE exhibited a slightly lower but acceptably high conductivity (3.22 mS cm^{-1}). It has been reported that the high polarity of SN can contribute to the fast transport of ions, although it is a relatively sluggish solvent compared with the carbonate electrolytes [30,36]. Interestingly, the addition of FEC had not effect on the ion conductivities of any of the electrolytes (the electrolytes containing FEC are shown as dotted lines in Fig. 1**e**). Notably, the ionic conductivities of the SNEs sharply decreased under 20 °C in contrast to those of the CLEs. This decrease is attributed to the phase transitions into the plastic-crystal, as demonstrated by the DSC analysis (Fig. 1**b**). In the plastic-crystal phase under 20 °C, SNFEC exhibited slightly higher conductivity than SNE because the presence of FEC reduced the structural regularity of SN [33]. Nevertheless, the ionic conductivities of SNE and SNFEC were sufficiently high, ~10^{-3} S cm^{-1} at RT, demonstrating the feasibility of their use in cells with Sn anodes.

In order to analyze their thermal stabilities, thermo-gravimetric analysis (TGA) was conducted, as shown in Fig. 1**f**. The temperature at which a sudden weight loss starts indicates the stability of a material against thermal decomposition. For the conventional electrolytes (CLE, CLEFEC, and CLE2), the first weight losses were responsible for DEC evaporations [37], and the subsequent declines are related to the thermal decompositions [38]. All the carbonate-based electrolytes reached only 50% of the weight at 150 °C. In contrast, the SNFEC electrolyte showed no particular change until 150 °C, indicating high thermal stability. Additionally, temperature-dependent viscosity (**Figure S2**) and contact angle test on the Sn electrode (**Figure S3**) are provided. Through

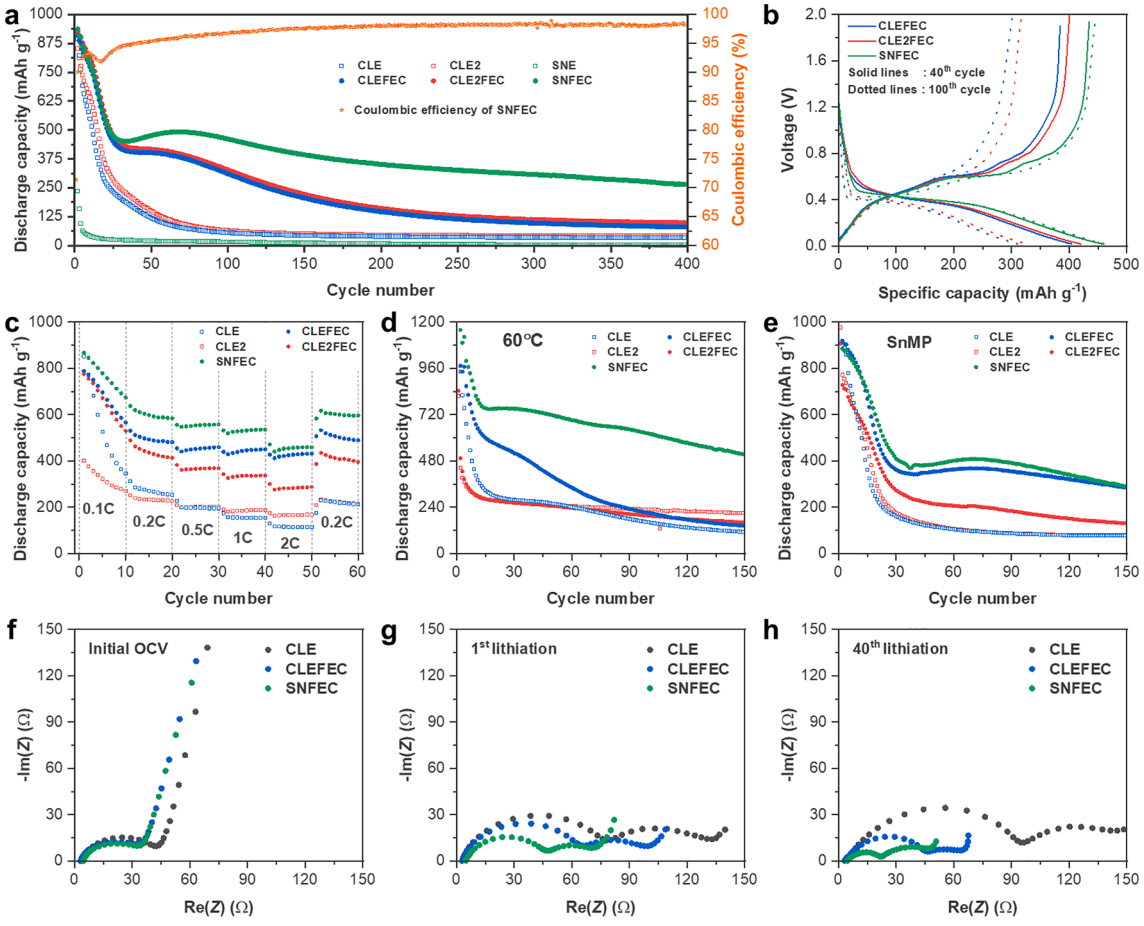

Fig. 2. Electrochemical performance of Sn (~150 nm) half-cells with various electrolytes. (a) Cyclabilities at constant rate of 0.2C at 30 °C and (b) corresponding galvanostatic charge and discharge profiles at 40th and 100th cycles. (c) Rate capability test at 30 °C and (d) cyclabilities at high temperature (60 °C). (e) Cyclabilities of SnMP (~10 μm) with various electrolytes at 30 °C. EIS results (f) at open-circuit voltage and (g) after 1st cycle and (h) 40th cycle in lithiated state.

the various analyses, it was concluded that SNFEC can provide acceptable ionic conductivity with high thermal stability and is suitable for application in a half-cell system with Li metal.

Fig. 2**a** shows the electrochemical performances of Sn electrodes in half-cells with various electrolytes at 30 °C. Nano-sized Sn particles with ~ 150 nm diameter were used because they are relatively resistant to particle cracking and deliver a reversible capacity [39]. In addition, the nano-sized particles could generate more SEI in large areas, which is a favorable condition to study the relationship between electrolyte engineering and SEI changes. As shown in Fig. 2**a**, the SNE cell exhibited the most inferior cycle stability because of the fast polymerization, as we demonstrated. The cells with the conventional electrolytes (CLE and CLE2) also showed very poor cycle stabilities. They quickly degraded because it was difficult for the organic-rich SEI to tolerate the serious pulverization of Sn particles. The addition of FEC (CLEFEC and CLE2FEC) resulted in slightly improved performances as the additive helped to form a rigid SEI layer on Sn, as previously reported [23,24]. Notably, the cell with SNFEC exhibited exceptional capacity retention. After 400 cycles, the discharge capacity of the SNFEC cell remained at 265 mAh g^{-1}, whereas that of the others was negligible. Detailed charge and discharge profiles and initial irreversible reaction are inscribed in **Figure S4 and S5a**. Although all the cells, regardless of the electrolytes, showed relatively low coulombic efficiencies (CEs) in the initial cycles, they were slowly recovered in continuing cycles. This result is attributed to the initial SEI formations affected by the volume changes of the active materials, as commonly observed in alloying materials [4,5]. The small bump near the 40th cycle is also attributed to the volume changes that occurred while progressing toward the "critical size" of the alloying particle [40,41].

Fig. 2**b** clearly shows the superior cycle stability of the SNFEC cell compared with that of the other CLE cells. The electrochemical profiles at the 40th and 100th cycles of SNFEC were almost identical, whereas the capacity retentions of CLEFEC and CLE2FEC were only approximately 76.8% and 77.8%, respectively. Detailed charge-discharge profiles at various cycle numbers are compared in **Figure S5**. In addition, to further investigate the significance of SNFEC, we performed the rate capability test at different current rates ranging from 0.1C to 2C at 30 °C (Fig. 2**c**). Before the rate capability test, all the cells were pre-cycled three times at 0.05C (**Figure S6**). Notably, the SNFEC cell showed superior performance at all the C-rates, implying that the combination of SN and FEC is effective in enhancing the electrochemical performance. Considering that the ion conductivities of CLEs are slightly higher than that of SNFEC (Fig. 1**e**), the superior rate capability of SNFEC was unexpected, and we describe this in terms of the different SEI conditions, which will be discussed later.

The cycle performances of Sn half-cells at the relatively high temperature of 60 °C were also compared (Fig. 2**d**). Surprisingly, the SNFEC cell exhibited the highest cycle stability, which is more obvious upon comparison with the cases at 30 °C. The superior cyclability at 60 °C is attributed to the high thermal stability of SN-based electrolytes, as we previously demonstrated (Fig. 1**f**). Although the high thermal stability of SN has been reported [33,35,42], its effect in alloying materials related to the SEI stability is demonstrated for the first time. Significant degradation of the CLE2FEC cell was observed at 60 °C (Fig. 2**d**) compared with that at 30 °C in Fig. 2**a**. This result is because the $LiPF_6$ salt produces thermally unstable SEI components such as LEDC [43], which decomposes at 55 °C into more complex species, critically damaging the formed SEI [44]. Additional comparisons of the cyclabilities at different temperatures of 45 °C and 70 °C are provided in **Figure S7**, demonstrating again that the use of SNFEC is advantageous

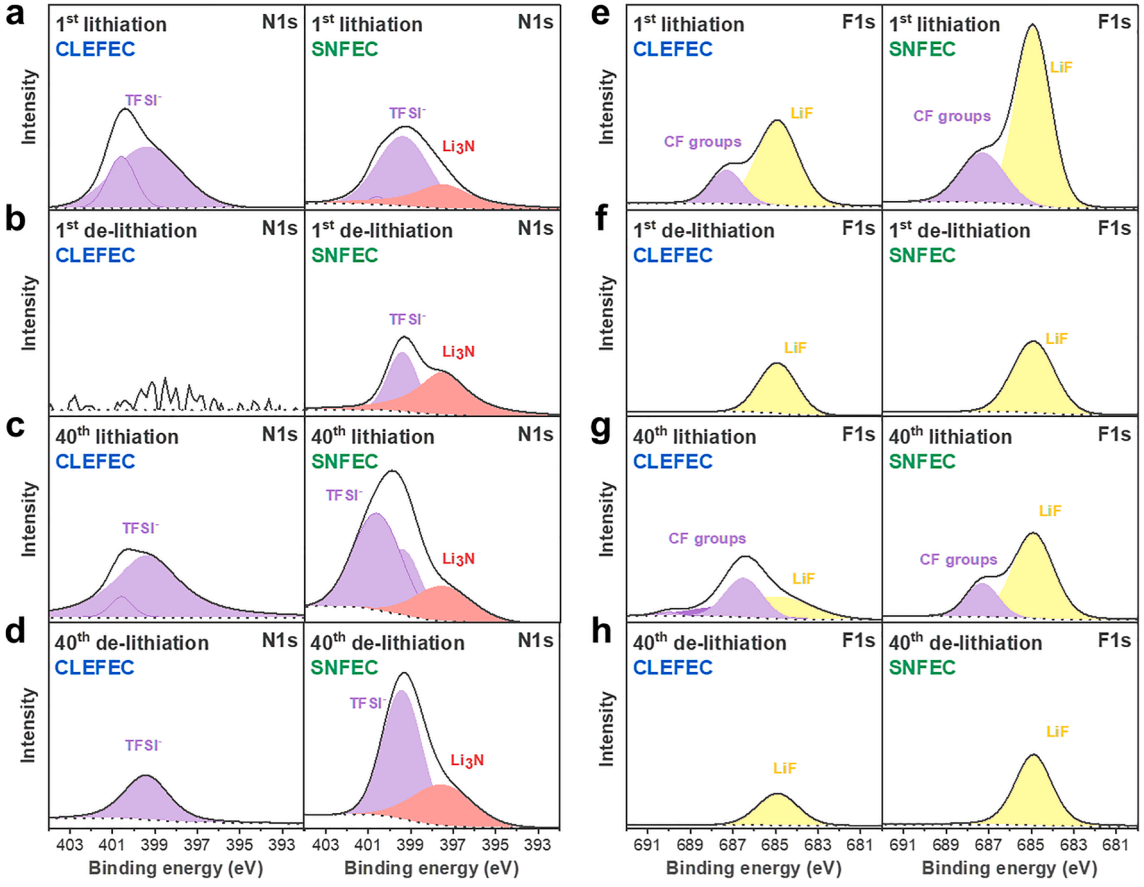

Fig. 3. XPS spectra of Sn electrodes cycled in CLEFEC and SNFEC electrolytes. (a–d) N 1 s and (e–h) F 1 s core-level energies of the electrode surfaces at 1st and 40th cycles.

under high-temperature conditions. We also prepared Sn electrodes with much larger particle sizes of ~ 10 μm diameter (SnMP) and investigated the effects of electrolyte engineering. Fig. 3**e** confirms that the SNFEC cell exhibited the highest cycle stability at 30 °C; however, the improvement was not significantly dominant compared with the result of nano-sized Sn. This finding is reasonable as the small particles could expose relatively larger surface areas directly faced with electrolyte, thus maximizing the effect of the SEI. On the other hand, SnMP could expose relatively small surface areas for the SEI; naturally, the effect of electrolyte engineering might not be significant. [41,45]

To investigate the effects of the electrolytes on the SEI properties, we conducted electrochemical impedance spectroscopy (EIS) analysis for Sn half-cells (Fig. 2**f–h**). After each cell assembly, the cell was relaxed for 12 hours, and EIS analysis was performed at an open-circuit voltage (OCV), as shown in Fig. 2**f**. The cells with FEC (CLEFEC and SNFEC) had relatively lower impedances than the bare CLE, implying that FEC contributed to the formation of a less-resistive film [33,46]. After the first lithiation (Fig. 2**g**), the Nyquist plots displayed distinct two semicircles, as similarly observed in typical alloying materials [47]. The first semicircle in the high-frequency region represents the SEI resistance (R_{SEI}), and the semicircle in the middle frequency corresponds to the charge-transfer resistance (R_{CT}) [47,48]. To distinguish the R_{SEI} values for the overlapped data, we fitted the EIS plot based on the equivalent circuit (**Figure S8a**), and the calculated R_{SEI} values are presented in a table in **Figure S8b**. The initially low resistances for the CLE, CLEFEC, and SNFEC cells at OCVs were increased after the first lithiation, which is attributed to the SEI formations on the lithiated Sn particles. R_{SEI} of the CLE cell showed a drastic increase, and that of the CLEFEC cell showed a relatively gentle increase upon cycling. However, they eventually increased substantially after the 40th lithiation (Fig. 2**h**), and much higher R_{SEI} values were measured after 400 cycles (**Figure S8b**). This result was observed because the organic-based SEI is sensitive to the dynamic volume changes and prone to lose its original SEI layer. Notably, the SNFEC cell could maintain the small resistances upon cycling and show the smallest value after the 40th lithiation and even after 400 cycles (**Figure S8b**). Additionally, in the de-lithiated states (**Figure S9a-c**), similar tendencies were observed, and the smallest R_{SEI} of the SNFEC cell was also proved. The outstanding impedance result of the SNFEC cell is likely associated with the SEI characteristics of the Sn particle, and a close surface analysis is needed to explain the synergistic effect of SN and FEC related to the SEI properties.

To directly investigate the SEI compositions, X-ray photoelectron spectroscopy (XPS) analysis was conducted. Comparison of the Sn electrodes cycled in CLEFEC (Sn-CLEFEC) and SNFEC (Sn-SNFEC) cells enabled determination of the effects of SN and FEC on the SEI quality. In the N 1 s spectra of the Sn-CLEFEC at the 1st lithiation (left images in Fig. 3**a–b**), only the peaks related to the LiTFSI salt were defined (399.4 and 400.5 eV) [49,50]. These organic-based SEI layers are certainly unstable as their signal disappeared after the 1st de-lithiation. Similar observations were made for the lithiation and de-lithiation processes of the 40th cycle (Fig. 3**c–d**), proving that it is difficult for the conventional electrolytes to respond to the dynamic volume changes accompanied by the unstable SEI layer. The undesired changes were more significant in the Sn SEI of the CLE cell without FEC (Sn-CLE), as shown in **Figure S10**. In contrast, distinct peaks of Li_3N at the binding energy of 397.5 eV were clearly observed for Sn-SNFEC (right images in Fig. 3**a–d**) [51]. It should be mentioned that the formation of Li_3N is one of important effects of SN because it can contribute to the formation of a stable and rigid SEI. Li_3N can act as a fast ionic conductor (10^{-3} S cm^{-1} at RT) [52], and its relatively high Young's modulus of 150 GPa (*e.g.* 58.1 GPa for LiF) is also advantageous to provide a mechanically safe and rigid shielding layer [11,53]. The great benefit of Li_3N as an SEI component has been reported elsewhere [54]. Notably, the generated Li_3N is stably maintained regardless of cycle numbers or states in the SNFEC cell. There have been a few reports dealing with the SN in terms of decomposition mechanism; (1) SN possessed both low LUMO (lowest unoccupied molecular orbital) and high HOMO (highest occupied molecular orbital) energies, reflecting the ability of preferential reduction and oxidation, respectively [55]. Therefore, SN could easily decompose into C≡N moieties which further reacts with electrolyte complex, resulting in the formation of Li_3N [56,57]. This agrees with another similar report on the nitrile decomposition [58]. (2) Other research described that the formation of surface SEI is based on the metal/ligand complexes with the nitrile (–CN) groups of SN [42].

In the F 1 s XPS spectra of Sn-CLEFEC (left images in Fig. 3**e–h**), two distinct peaks of LiF (684.9 eV) and CF groups (687.3 eV) were observed. The CF groups originated from the FEC decomposition[46] and are dependent on the cycle states. They clearly appeared in the lithiated state and disappeared in the de-lithiated state, implying the dynamic SEI changes [59]. In addition, the peak of inorganic LiF from the reduction of FEC underwent relatively fewer changes between the 1st lithiation and de-lithiation processes. However, after multiple cycles, the repeated Sn pulverizations and continuous exposures of fresh surfaces eventually degraded the initially formed LiF [29]. Thus, at the 40th cycle (left in Fig. 4**g, h**), the LiF intensities were relatively weakened compared with those at the 1st cycle. This result indicates that the FEC additive is insufficient to maintain the original SEI in the alloying materials. In contrast, the intensities of the LiF peaks of Sn-SNFEC (right images in Fig. 3**e–h**) were higher than those of their Sn-CLEFEC counterparts, and the overall high intensities were well preserved upon cycling. This result indicates that the inorganic LiF is more stably maintained with the support of SN. The XPS surface wide scan (**Figure S11**) further supports the idea that the unstable organic compounds (oxygen-containing species) were greatly evolved after the cycles in Sn-CLEFEC compared with in Sn-SNFEC. In short, SNFEC can effectively prevent the accumulation of unstable organic species, instead forming the key inorganic component of Li_3N as well as helping to preserve LiF during cycles.

To attain a deeper understanding of the SEI properties, the XPS depth-profile atomic concentrations were measured at the 40th lithiation states. Fig. 4a displays the relative concentrations of F, N, and O elements, which can provide clues for estimating the quantitative amounts of LiF, Li_3N, and LEDC, respectively. When comparing the F atomic concentrations, Sn-SNFEC (F green line) contained relatively abundant inorganic LiF (16.16%) at the surface (0 nm), whereas the Sn-CLE (F red line) contained the smallest concentration (3.79%). In the inner depths, the gap was still observed, demonstrating that the LiF was well preserved with the help of SN in the SNFEC cell. The N concentration showed a similar tendency; the N concentrations decreased in the SNFEC, CLEFEC, and CLE cells in that order. This result proves that the Sn-SNFEC contained much more Li_3N inorganic species in the SEI layer than the Sn-CLE and Sn-CLEFEC. In contrast, the concentrations of oxygen species were in complete reverse order. Sn-CLE (O red line) contained the highest oxygen content, whereas Sn-SNFEC (O green line) contained the lowest oxygen content. The tendencies of the depth profiles were almost the same with the de-lithiated state (**Figure S12**). These results demonstrate that the SEI layer in Sn-SNFEC was mainly composed of inorganics (LiF and Li_3N), whereas Sn-CLE contained the oxygen-rich SEI layer.

To support our XPS results, time-of-flight secondary ion mass spectrometry (TOF-SIMS) analysis was conducted. Fig. 4**b** presents the normalized intensities for target species at the Sn electrode surfaces in the three different cells. Relatively higher intensities of LiO^-, C_3H^-, and C_2HO^- species were observed for the Sn surfaces (0 to 25 nm regions, outer SEI layer) in Sn-CLE and Sn-CLEFEC than for Sn-SNFEC. The C_3H^-, and C_2HO^- components are major contributors to the unstable organic SEI [54,60], and these results are consistent with our XPS results. In addition, evidence of the LiF component at the inner SEI layer could be obtained by tracing the LiF_2^-. LiF_2^- fragments were detectable in wide ranges of depth for Sn-SNFEC; in contrast, its intensity was relatively lower in Sn-CLEFEC and almost negligible in Sn-CLE. It should be noted that the LiN^- fragment (indicator of Li_3N) signals showed similar distributions with LiF_2^-; the highest LiN^- content was detected particularly

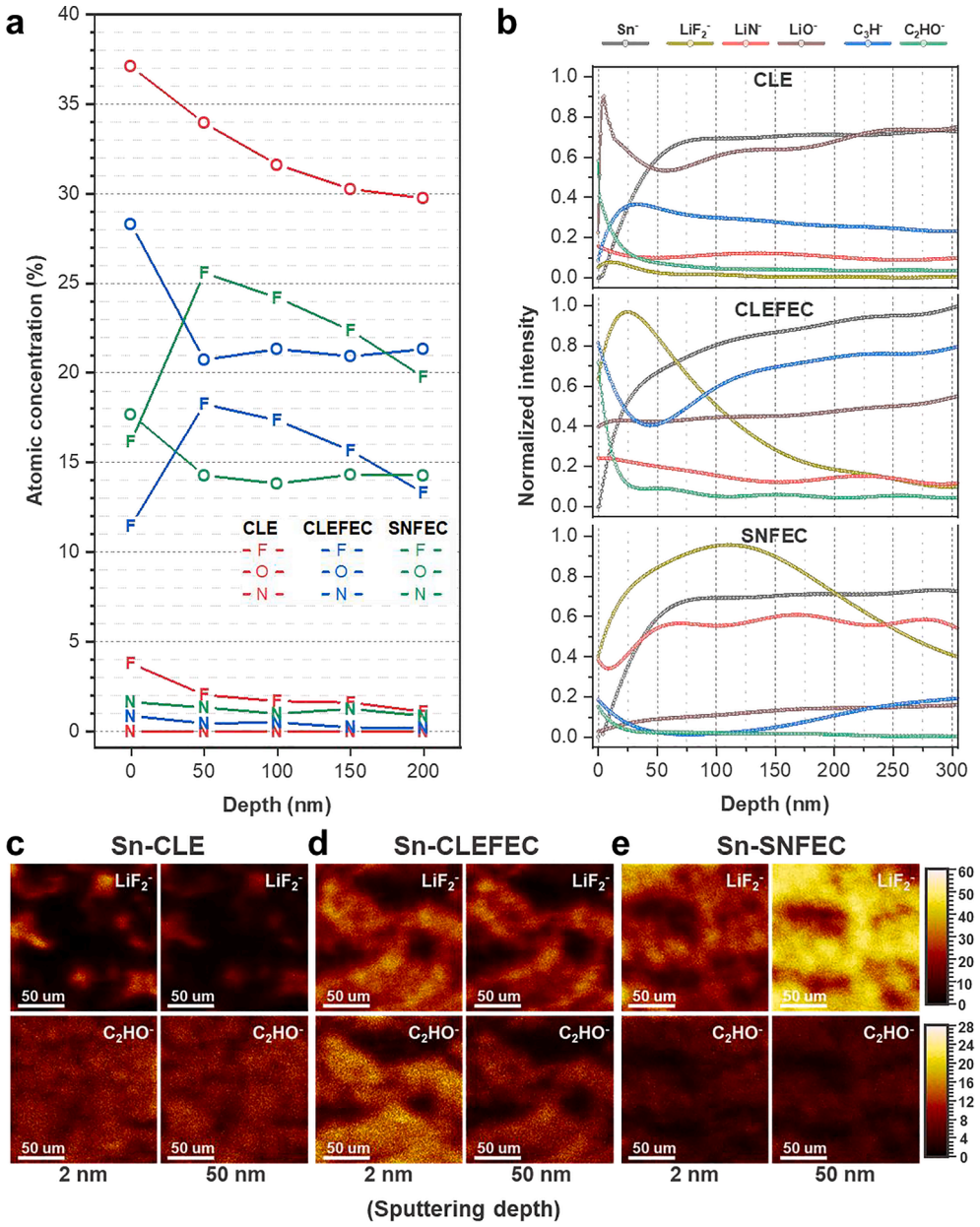

Fig. 4. Elemental depth profiles for Sn electrodes after 40th lithiation with different electrolytes. (a) XPS concentration depth profiles for F, O, and N elements. (b) TOF-SIMS analyses with negative polarities. Two-dimensional TOF-SIMS images of targeted species in (c) Sn-CLE, (d) Sn-CLEFEC, and (e) Sn-SNFEC after 2 nm and 50 nm depth sputtering.

in Sn-SNFEC, and the lowest was detected in Sn-CLE. The TOF-SIMS results demonstrate again that in the SNFEC cell, the SEI is mainly composed of the inorganics LiF and Li_3N, whereas in the CLE cell, the SEI is mostly composed of organic species.

The distributions of the species of interest were investigated using 2D surface images with chemical mapping, which were taken at the specific sputtering depths of 2 and 50 nm (Fig. 4**c–e**). The 2 nm sputtering represents the very outer surface of the Sn electrode, whereas 50 nm corresponds to the relatively inner side of the SEI. The LiF_2^- mapping image shows that the concentration became denser in the order of Sn-CLE (Fig. 4**c**), Sn-CLEFEC (Fig. 4**d**), and Sn-SNFEC (Fig. 4**e**). LiF was dominant in the Sn-SNFEC regardless of the sputtering time. This result confirms that the dense LiF film could be well generated in SEI layers by the support of SN. In reverse, the mapping images of C_2HO^- show that the Sn-CLE and Sn-CLEFEC contain more C_2HO^- compared with Sn-SNFEC. Based on the results of the XPS and TOF-SIMS analyses, it was concluded that the SNFEC could produce an inorganic-based SEI mainly composed of LiF and Li_3N, which are advantageous for the formation of a mechanically rigid and chemically stable layer. To directly observe the quality of SEI layer on Sn electrode affected by the different electrolytes (CLEFEC and SNFEC), transmission electron microscopy (TEM) analysis was performed (**Figure S13**). The results of these analyses could explain how the SNFEC cell delivered improved electrochemical properties.

A summary of the effects of the SNFEC electrolyte based on the various surface analyses is presented in Fig. 5. Through the comprehensive investigations, we confirmed that the properties of the SEI layer of Sn electrode are highly dependent on the electrolyte selected. Conventional carbonate electrolytes, particularly EC, produce mainly organic components in the SEI, and the mechanically weak layer is prone to dissolve and undergoes continuous degradation during cycling (top route in Fig. 5). In contrast, SNFEC can produce a dense inorganic-rich SEI, mainly dominated by LiF and Li_3N (bottom section in Fig. 5). It

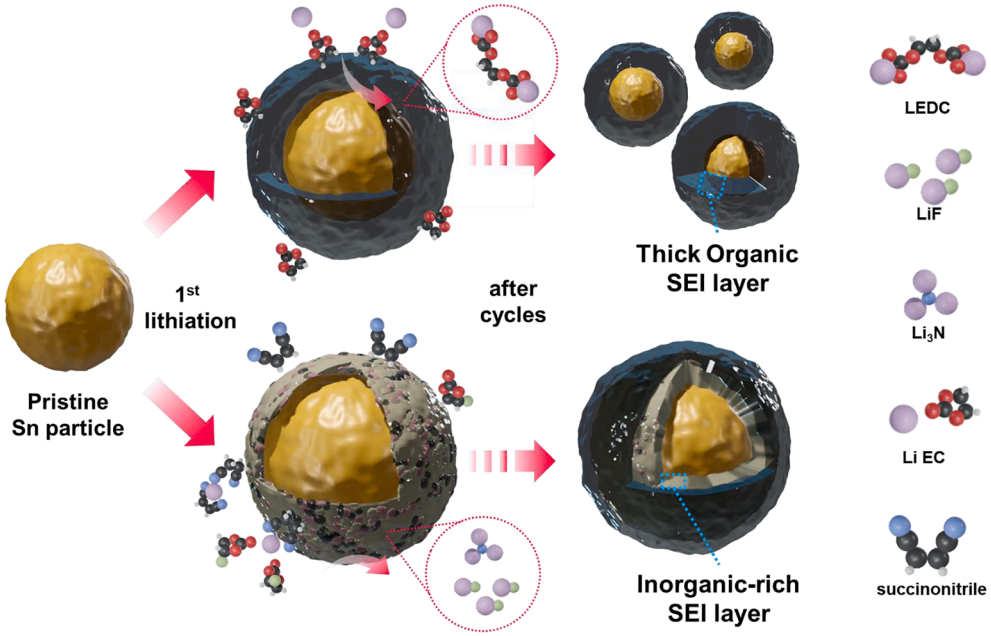

Fig. 5. Schematic illustration of Sn particle and its SEI evolution in (top) conventional carbonate-based electrolyte and (bottom) SNFEC electrolyte.

should be noted that the Sn particles experience huge volume expansion during lithiation. Considering the intrinsic behavior of LiF [61], and a competitive reaction with the electrolyte components on the newly exposed particle surface, the solely use of FEC is not enough to well preserve the original surface film (SEI). The orbital theory can estimate which component could preferentially form at the Sn electrode surface, and SN in electrolyte complex is known to possess the lower LUMO energy [55,56]. Therefore, during the electrochemical reduction (Sn lithiation), Li_3N from the SN decomposition could be preferentially generated [55,57]. SN reduction is expected to preferentially take place rather than undesired organic species; thus it helps to maintain the structure of inner SEI as well as to support the regenerated LiF on the newly exposed Sn surface. On the other hand, in the case of CLEFEC, unstable organic SEI layer is expected to form a rough surface, resulting in an irregular morphology of SEI layer.

In the SNFEC electrolyte system, FEC and SN have a synergistic effect for improving the electrochemical performance of the Sn electrode. LiF from FEC plays an important role as a mechanical support in SEI, alleviating the volume expansion and rapid pulverization while protecting Li metal from the side reaction of SN polymerization. The replacement of carbonate-based solvents with SN can also remarkably enhance the cell cycling stability. SN restricts the formation of unstable organic species, instead forming favorable Li_3N as well as support to preserve LiF, leading to the formation of a dense inorganic SEI layer. This simple electrolyte engineering drives the formation of a favorable SEI, resulting in improved cyclability with excellent thermal stability.

3. Conclusion

To solve the prevailing problem of the unstable SEI of Sn alloying anode, we adopted a new electrolyte system by combining SN and FEC (SNFEC). The effects of electrolyte engineering on the SEI properties in terms of electrochemical performance were also investigated. This simple approach can effectively prevent the formation of vulnerable organic compounds usually generated in conventional carbonate electrolytes, and instead, trigger the formation of a dense inorganic-rich SEI layer. By adopting the SN and FEC electrolytes, the SEI compounds of Sn can be tuned into favorable inorganics, mainly LiF supported by Li_3N, which are ideal products as the SEI because they are insoluble, mechanically robust, and fast ion-conducting. The inorganic SEI is demonstrated to effectively buffer the large volume expansion, leading to improved cyclability with higher energy efficiency. The changes of the SEI layer affected by the electrolyte were analyzed using various surface analysis techniques, and the individual effects of SN and FEC on the electrochemical performance were discussed. This study explores the practical applications of the eutectic SN in divergent LIB systems, providing useful insight into future electrolyte design.

4. Experimental

4.1. Electrolytes and cell preparations

To synthesize the SN-based electrolyte, pure SN purchased from Sigma-Aldrich (99%) was vacuum dried at 90 °C overnight. The pure SN was mixed with 1 M LiTFSI and stirred overnight to obtain the succinonitrile electrolyte (SNE). To produce the succinonitrile electrolyte with FEC (SNFEC), 5 wt% FEC (99%, Aldrich) additive was additionally added to the prepared SNE. As control samples, conventional commercial liquid electrolytes with different Li salts such as LiTFSI (CLE) and $LiPF_6$ (CLE2) in EC:DEC (1:1 vol) were synthesized using the same procedure. All of the procedures were carefully conducted in a dry room (dew point − 70 °C, max. moisture less than 5%). The commercial Sn powders with nano-sized (150 nm) and micro-sized (10 μm) particles were purchased from Sigma-Aldrich. To fabricate the Sn electrode, each Sn powder was mixed with carbon black and polyacrylic acid (PAA, Mv = 350000, Aldrich) binder in ethanol in a 7:2:1 ratio. The slurry was cast on copper foil with a thickness set to 0.1 mm and dried at 80 °C overnight. The prepared electrode was punched into a diameter of 1.2 cm, with an average loading mass of approximately 0.8–1.1 mg cm^{-2}. Each Sn electrode was assembled in a coin-type (2032) cell with a glass fiber (Whatman) separator, Li metal counter electrode, and 100 μL of the electrolyte.

4.2. Analyses and characterization

Bonding analyses for the prepared SN-based electrolyte were conducted using Fourier-transform infrared spectroscopy (FT-IR, Perkin Elmer, Spectrum 100 FT-IR). To estimate the thermal properties, DSC (TA Instruments Auto Q20) from −50 to 75 °C in a N_2 atmosphere and TGA from 30 to 250 °C in and argon atmosphere were performed. The

surface chemical composition was characterized using XPS (VersaProbe Ulvac-PHI, Japan) with monochromated Al Ka (1486.6 eV). The XPS depth profile was also obtained with Ar sputtering after 0, 2, 4, 6, and 8 min. ION-TOF (Münster, Germany) was used for TOF-SIMS studies. The depth profile for each component was analyzed in negative polarity mode, with primary Bi_3^+ gun (30 keV) in a raster area of 50 × 50 μm after sputtering with secondary Cs^+ gun (3 keV) at a calculated sputter rate of 0.2958 nm s^{-1} (as pure Li material). The 2D images (150 μm × 150 μm size) were taken after 2 and 50 nm of depth sputtering. Before the XPS and TOF-SIMS analyses, the cycled Sn electrodes were washed with dimethyl carbonate (DMC) and dried in an argon-filled glovebox; they were carefully transferred with an airtight holder for all the experiments.

4.3. Electrochemical tests

The electrochemical performances were tested using a potentio-galvanostat cycler (WBCS3000S, WonATech). The cell cyclability and galvanostatic charge–discharge profile were measured in the voltage range between 0.02 and 2 V vs. Li at a constant current density (0.2C) under different temperatures (30, 45, 60, and 70 °C). Rate capability tests were performed at altered rate conditions; the initial 3 cycles were performed at 0.05C, then constantly increased until 2C (10 cycles). The ionic conductivities of the electrolytes were measured using EIS (Bio-logic VSP-300) between 1 MHz and 50 mHz with 10-mV AC perturbation in a blocking-cell configuration.

Declaration of Competing Interest

The authors declare that they have no known competing financial interests or personal relationships that could have appeared to influence the work reported in this paper.

Acknowledgments

This research was supported by KIST Institutional Program (No. 2E31001) and the Development Program of Core Industrial Technology (No. 20012318) funded by the Ministry of Trade, Industry & Energy; the Technology Development Program to Solve Climate Changes of the National Research Foundation (NRF), funded by the Ministry of Science & ICT of Korea (2017M1A2A2044482).

Appendix A. Supplementary data

Supplementary data to this article can be found online at https://doi.org/10.1016/j.cej.2021.130524.

References

[1] N. Nitta, G. Yushin, High-capacity anode materials for lithium-ion batteries: choice of elements and structures for active particles, Part. Part. Syst. Charact. 31 (3) (2014) 317–336, https://doi.org/10.1002/ppsc.201300231.
[2] M.T. McDowell, S.W. Lee, W.D. Nix, Y. Cui, 25th anniversary article: understanding the lithiation of silicon and other alloying anodes for lithium-ion batteries, Adv. Mater. 25 (36) (2013) 4966–4985, https://doi.org/10.1002/adma.201301795.
[3] D. Liu, Z. Liu, X. Li, W. Xie, Q. Wang, Q. Liu, Y. Fu, D. He, Group IVA element (Si, Ge, Sn)-based alloying/dealloying anodes as negative electrodes for full-cell lithium-ion batteries, Small 13 (45) (2017) 1702000, https://doi.org/10.1002/smll.201702000.
[4] F. Xin, M.S. Whittingham, Challenges and Development of Tin-Based Anode with High Volumetric Capacity for Li-Ion Batteries, EER 3 (4) (2020) 643–655, https://doi.org/10.1007/s41918-020-00082-3.
[5] W. Li, X. Sun, Y. Yu, Si-, Ge-, Sn-based anode materials for lithium-ion batteries: From structure design to electrochemical performance, Small Methods 1 (3) (2017) 1600037, https://doi.org/10.1002/smtd.201600037.
[6] S. Chae, M. Ko, K. Kim, K. Ahn, J. Cho, Confronting issues of the practical implementation of Si anode in high-energy lithium-ion batteries, Joule 1 (1) (2017) 47–60, https://doi.org/10.1016/j.joule.2017.07.006.
[7] X. Meng, Y. Xu, H. Cao, X. Lin, P. Ning, Y. Zhang, Y.G. Garcia, Z. Sun, Internal failure of anode materials for lithium batteries — A critical review, GEE 5 (1) (2020) 22–36, https://doi.org/10.1016/j.gee.2019.10.003.
[8] I. Hasa, A.M. Haregewoin, L. Zhang, W.-Y. Tsai, J. Guo, G.M. Veith, P.N. Ross, R. Kostecki, Electrochemical reactivity and passivation of silicon thin-film electrodes in organic carbonate electrolytes, ACS Appl. Mater. Interfaces 12 (36) (2020) 40879–40890, https://doi.org/10.1021/acsami.0c09384.
[9] S.-P. Kim, A.C.T.v. Duin, V.B. Shenoy, Effect of electrolytes on the structure and evolution of the solid electrolyte interphase (SEI) in Li-ion batteries: A molecular dynamics study, J. Power Sources 196 (20) (2011) 8590–8597, https://doi.org/10.1016/j.jpowsour.2011.05.061.
[10] S.K. Heiskanen, J. Kim, B.L. Lucht, Generation and evolution of the solid electrolyte interphase of lithium-ion batteries, Joule 3 (10) (2019) 2322–2333, https://doi.org/10.1016/j.joule.2019.08.018.
[11] H. Shin, J. Park, S. Han, A.M. Sastry, W. Lu, Component-/structure-dependent elasticity of solid electrolyte interphase layer in Li-ion batteries: Experimental and computational studies, J. Power Sources 277 (2015) 169–179, https://doi.org/10.1016/j.jpowsour.2014.11.120.
[12] H. Wu, H. Jia, C. Wang, J.-G. Zhang, W. Xu, Recent progress in understanding solid electrolyte interphase on lithium metal anodes, Adv. Energy Mater. 11 (5) (2021) 2003092, https://doi.org/10.1002/aenm.202003092.
[13] L. Wang, A. Menakath, F. Han, Y. Wang, P.Y. Zavalij, K.J. Gaskell, O. Borodin, D. Iuga, S.P. Brown, C. Wang, K. Xu, B.W. Eichhorn, Identifying the components of the solid–electrolyte interphase in Li-ion batteries, Nat. Chem. 11 (9) (2019) 789–796, https://doi.org/10.1038/s41557-019-0304-z.
[14] P. Lu, C. Li, E.W. Schneider, S.J. Harris, Chemistry, impedance, and morphology evolution in solid electrolyte interphase films during formation in lithium ion batteries, J. Phys. Chem. C 118 (2) (2014) 896–903, https://doi.org/10.1021/jp4111019.
[15] E. Peled, S. Menkin, SEI: Past, present and future, J. Electrochem. Soc. 164 (7) (2017) A1703, https://doi.org/10.1149/2.1441707jes.
[16] B. Wang, B. Luo, X. Li, L. Zhi, The dimensionality of Sn anodes in Li-ion batteries, Mater. Today 15 (12) (2012) 544–552, https://doi.org/10.1016/S1369-7021(13)70012-9.
[17] J. Liu, X.i. Chen, J. Kim, Q. Zheng, H. Ning, P. Sun, X. Huang, J. Liu, J. Niu, P. V. Braun, High volumetric capacity three-dimensionally sphere-caged secondary battery anodes, Nano Lett. 16 (7) (2016) 4501–4507, https://doi.org/10.1021/acs.nanolett.6b01711.
[18] L. Liu, F. Xie, J. Lyu, T. Zhao, T. Li, B.G. Choi, Tin-based anode materials with well-designed architectures for next-generation lithium-ion batteries, J. Power Sources 321 (2016) 11–35, https://doi.org/10.1016/j.jpowsour.2016.04.105.
[19] K. Schroder, J. Alvarado, T.A. Yersak, J. Li, N. Dudney, L.J. Webb, Y.S. Meng, K. J. Stevenson, The effect of fluoroethylene carbonate as an additive on the solid electrolyte interphase on silicon lithium-ion electrodes, Chem. Mater. 27 (16) (2015) 5531–5542, https://doi.org/10.1021/acs.chemmater.5b01627.
[20] X.-Q. Zhang, X.-B. Cheng, X. Chen, C. Yan, Q. Zhang, Fluoroethylene carbonate additives to render uniform Li deposits in lithium metal batteries, Adv. Funct. Mater. 27 (10) (2017) 1605989, https://doi.org/10.1002/adfm.201605989.
[21] E. Markevich, G. Salitra, D. Aurbach, Fluoroethylene carbonate as an important component for the formation of an effective solid electrolyte interphase on anodes and cathodes for advanced li-ion batteries, ACS Energy Lett. 2 (6) (2017) 1337–1345, https://doi.org/10.1021/acsenergylett.7b00163.
[22] Z. Zhu, Y. Tang, Z. Lv, J. Wei, Y. Zhang, R. Wang, W. Zhang, H. Xia, M. Ge, X. Chen, Fluoroethylene carbonate enabling a robust LiF-rich solid electrolyte interphase to enhance the stability of the MoS2 anode for lithium-ion storage, Angew. Chem. Int. Ed. 57 (14) (2018) 3656–3660, https://doi.org/10.1002/anie.201712907.
[23] K. Eom, J. Jung, J.T. Lee, V. Lair, T. Joshi, S.W. Lee, Z. Lin, T.F. Fuller, Improved stability of nano-Sn electrode with high-quality nano-SEI formation for lithium ion battery, Nano Energy 12 (2015) 314–321, https://doi.org/10.1016/j.nanoen.2014.12.041.
[24] S. Hong, M.-H. Choo, Y.H. Kwon, J.Y. Kim, S.-W. Song, Mechanisms for stable solid electrolyte interphase formation and improved cycling stability of tin-based battery anode in fluoroethylene carbonate-containing electrolyte, Adv. Mater. Interfaces 3 (22) (2016) 1600172, https://doi.org/10.1002/admi.201600172.
[25] C. Shen, S. Wang, Y. Jin, W.-Q. Han, In situ AFM imaging of solid electrolyte interfaces on HOPG with ethylene carbonate and fluoroethylene carbonate-based electrolytes, ACS Appl. Mater. Interfaces 7 (45) (2015) 25441–25447, https://doi.org/10.1021/acsami.5b08238.
[26] N.-S. Choi, K.H. Yew, K.Y. Lee, M. Sung, H. Kim, S.-S. Kim, Effect of fluoroethylene carbonate additive on interfacial properties of silicon thin-film electrode, J. Power Sources 161 (2) (2006) 1254–1259, https://doi.org/10.1016/j.jpowsour.2006.05.049.
[27] Y. Jin, N.-J. Kneusels, P.C.M.M. Magusin, G. Kim, E. Castillo-Martínez, L. E. Marbella, R.N. Kerber, D.J. Howe, S. Paul, T. Liu, C.P. Grey, Identifying the structural basis for the increased stability of the solid electrolyte interphase formed on silicon with the additive fluoroethylene carbonate, J. Am. Chem. Soc. 139 (42) (2017) 14992–15004, https://doi.org/10.1021/jacs.7b06834.
[28] F.A. Soto, Y. Ma, J.M. Martinez de la Hoz, J.M. Seminario, P.B. Balbuena, Formation and growth mechanisms of solid-electrolyte interphase layers in rechargeable batteries, Chem. Mater. 27 (23) (2015) 7990–8000, https://doi.org/10.1021/acs.chemmater.5b03358.
[29] A. Wang, S. Kadam, H. Li, S. Shi, Y. Qi, Review on modeling of the anode solid electrolyte interphase (SEI) for lithium-ion batteries, Npj Comput. Mater 4 (1) (2018) 15, https://doi.org/10.1038/s41524-018-0064-0.
[30] P.-J. Alarco, Y. Abu-Lebdeh, A. Abouimrane, M. Armand, The plastic-crystalline phase of succinonitrile as a universal matrix for solid-state ionic conductors, Nat. Mater. 3 (7) (2004) 476–481, https://doi.org/10.1038/nmat1158.
[31] Z. Hu, F. Xian, Z. Guo, C. Lu, X. Du, X. Cheng, S. Zhang, S. Dong, G. Cui, L. Chen, Nonflammable Nitrile Deep Eutectic Electrolyte Enables High-Voltage Lithium

Metal Batteries, Chem. Mater. 32 (8) (2020) 3405–3413, https://doi.org/10.1021/acs.chemmater.9b05003.
[32] F. Xian, J. Li, Z. Hu, Q. Zhou, C. Wang, C. Lu, Z. Zhang, S. Dong, C. Mou, G. Cui, Investigation of the cathodic interfacial stability of a nitrile electrolyte and its performance with a high-voltage LiCoO2 cathode, Chem. Commun. 56 (37) (2020) 4998–5001, https://doi.org/10.1039/D0CC00049C.
[33] Q. Zhang, K. Liu, F. Ding, W. Li, X. Liu, J. Zhang, Safety-reinforced succinonitrile-based electrolyte with interfacial stability for high-performance lithium batteries, ACS Appl. Mater. Interfaces 9 (35) (2017) 29820–29828, https://doi.org/10.1021/acsami.7b09119.
[34] M.B. Effat, Z. Lu, A. Belotti, J. Yu, Y.-Q. Lyu, F. Ciucci, Towards succinonitrile-based lithium metal batteries with long cycle life: The influence of fluoroethylene carbonate loading and the separator, J. Power Sources 436 (2019) 226802, https://doi.org/10.1016/j.jpowsour.2019.226802.
[35] C. Fu, Y. Ma, S. Lou, C. Cui, L. Xiang, W. Zhao, P. Zuo, J. Wang, Y. Gao, G. Yin, A dual-salt coupled fluoroethylene carbonate succinonitrile-based electrolyte enables Li-metal batteries, J. Mater. Chem. A 8 (4) (2020) 2066–2073, https://doi.org/10.1039/C9TA11341J.
[36] L.-Z. Fan, Y.-S. Hu, A.J. Bhattacharyya, J. Maier, Succinonitrile as a versatile additive for polymer electrolytes, Adv. Funct. Mater. 17 (15) (2007) 2800–2807, https://doi.org/10.1002/adfm.200601070.
[37] C. Arbizzani, G. Gabrielli, M. Mastragostino, Thermal stability and flammability of electrolytes for lithium-ion batteries, J. Power Sources 196 (10) (2011) 4801–4805, https://doi.org/10.1016/j.jpowsour.2011.01.068.
[38] C.L. Campion, W. Li, W.B. Euler, B.L. Lucht, B. Ravdel, J.F. DiCarlo, R. Gitzendanner, K. Abraham, Suppression of toxic compounds produced in the decomposition of lithium-ion battery electrolytes, Electrochem. Solid-State Lett. 7 (7) (2004) A194, https://doi.org/10.1149/1.1738551.
[39] X.H. Liu, L. Zhong, S. Huang, S.X. Mao, T. Zhu, J.Y. Huang, Size-dependent fracture of silicon nanoparticles during lithiation, ACS Nano 6 (2) (2012) 1522–1531, https://doi.org/10.1021/nn204476h.
[40] H. Kim, M. Seo, M.-H. Park, J. Cho, A Critical size of silicon nano-anodes for lithium rechargeable batteries, Angew. Chem. Int. Ed. 49 (12) (2010) 2146–2149, https://doi.org/10.1002/anie.200906287.
[41] M. Ashuri, Q. He, L.L. Shaw, Silicon as a potential anode material for Li-ion batteries: where size, geometry and structure matter, Nanoscale 8 (1) (2016) 74–103, https://doi.org/10.1039/C5NR05116A.
[42] Y.-S. Kim, T.-H. Kim, H. Lee, H.-K. Song, Electronegativity-induced enhancement of thermal stability by succinonitrile as an additive for Li ion batteries, Energy Environ. Sci. 4 (10) (2011) 4038–4045, https://doi.org/10.1039/C1EE01272J.
[43] M. Nie, B.L. Lucht, Role of Lithium Salt on Solid Electrolyte Interface (SEI) Formation and Structure in Lithium Ion Batteries, J. Electrochem. Soc. 161 (6) (2014) A1001–A1006, https://doi.org/10.1149/2.054406jes.
[44] T. Yoon, M.S. Milien, B.S. Parimalam, B.L. Lucht, Thermal decomposition of the solid electrolyte interphase (SEI) on silicon electrodes for lithium ion batteries, Chem. Mater. 29 (7) (2017) 3237–3245, https://doi.org/10.1021/acs.chemmater.7b00454.
[45] S. Huang, L.-Z. Cheong, S. Wang, D. Wang, C. Shen, In-situ study of surface structure evolution of silicon anodes by electrochemical atomic force microscopy, Appl. Surf. Sci. 452 (2018) 67–74, https://doi.org/10.1016/j.apsusc.2018.05.020.
[46] G.M. Veith, M. Doucet, R.L. Sacci, B. Vacaliuc, J.K. Baldwin, J.F. Browning, Determination of the solid electrolyte interphase structure grown on a silicon electrode using a fluoroethylene carbonate additive, Sci. Rep. 7 (1) (2017) 6326, https://doi.org/10.1038/s41598-017-06555-8.
[47] J. Guo, A. Sun, X. Chen, C. Wang, A. Manivannan, Cyclability study of silicon–carbon composite anodes for lithium-ion batteries using electrochemical impedance spectroscopy, Electrochim. Acta 56 (11) (2011) 3981–3987, https://doi.org/10.1016/j.electacta.2011.02.014.
[48] W. Choi, H.-C. Shin, J.M. Kim, J.-Y. Choi, W.-S. Yoon, Modeling and applications of electrochemical impedance spectroscopy (EIS) for lithium-ion batteries, J. Electrochem. Sci. Technol 11 (1) (2020) 1–13, https://doi.org/10.33961/jecst.2019.00528.
[49] S. Leroy, H. Martinez, R. Dedryvère, D. Lemordant, D. Gonbeau, Influence of the lithium salt nature over the surface film formation on a graphite electrode in Li-ion batteries: An XPS study, Appl. Surf. Sci. 253 (11) (2007) 4895–4905, https://doi.org/10.1016/j.apsusc.2006.10.071.
[50] Q. Wang, Z. Yao, C. Zhao, T. Verhallen, D.P. Tabor, M. Liu, F. Ooms, F. Kang, A. Aspuru-Guzik, Y.-S. Hu, M. Wagemaker, B. Li, Interface chemistry of an amide electrolyte for highly reversible lithium metal batteries, Nat. Commun. 11 (1) (2020) 4188, https://doi.org/10.1038/s41467-020-17976-x.
[51] Z. Lu, J. Yu, J. Wu, M.B. Effat, S.C.T. Kwok, Y. Lyu, M.M.F. Yuen, F. Ciucci, Enabling room-temperature solid-state lithium-metal batteries with fluoroethylene carbonate-modified plastic crystal interlayers, Energy Storage Mater. 18 (2019) 311–319, https://doi.org/10.1016/j.ensm.2018.08.021.
[52] U.v. Alpen, A. Rabenau, G. Talat, Ionic conductivity in Li3N single crystals, App. Phys. Lett. 30 (12) (1977) 621–623, https://doi.org/10.1063/1.89283.
[53] X. Li, F.E. Kersey-Bronec, J. Ke, J.E. Cloud, Y. Wang, C. Ngo, S. Pylypenko, Y. Yang, Study of lithium silicide nanoparticles as anode materials for advanced lithium ion batteries, ACS Appl. Mater. Interfaces 9 (19) (2017) 16071–16080, https://doi.org/10.1021/acsami.6b16773.
[54] H.-H. Sun, A. Dolocan, J.A. Weeks, R. Rodriguez, A. Heller, C.B. Mullins, In situ formation of a multicomponent inorganic-rich SEI layer provides a fast charging and high specific energy Li-metal battery, J. Mater. Chem. A 7 (30) (2019) 17782–17789, https://doi.org/10.1039/C9TA05063A.
[55] Q. Zhang, K. Liu, F. Ding, W. Li, X. Liu, J. Zhang, Enhancing the high voltage interface compatibility of LiNi0.5Co0.2Mn0.3O2 in the succinonitrile-based electrolyte, Electrochim. Acta 298 (2019) 818–826, https://doi.org/10.1016/j.electacta.2018.12.104.
[56] R. Chen, F. Liu, Y. Chen, Y. Ye, Y. Huang, F. Wu, L. Li, An investigation of functionalized electrolyte using succinonitrile additive for high voltage lithium-ion batteries, J. Power Sources 306 (2016) 70–77, https://doi.org/10.1016/j.jpowsour.2015.10.105.
[57] C. Wang, X. Sun, L.i. Yang, D. Song, Y. Wu, T. Ohsaka, F. Matsumoto, J. Wu, In situ ion-conducting protective layer strategy to stable lithium metal anode for all-solid-state sulfide-based lithium metal batteries, Adv. Mater. Interfaces 8 (1) (2021) 2001698, https://doi.org/10.1002/admi.202001698.
[58] J. Sun, C. He, X. Yao, A. Song, Y. Li, Q. Zhang, C. Hou, Q. Shi, H. Wang, Hierarchical composite-solid-electrolyte with high electrochemical stability and interfacial regulation for boosting ultra-stable lithium batteries, Adv. Funct. Mater. 31 (1) (2021) 2006381, https://doi.org/10.1002/adfm.202006381.
[59] H. Bryngelsson, M. Stjerndahl, T. Gustafsson, K. Edström, How dynamic is the SEI? J. Power Sources 174 (2) (2007) 970–975, https://doi.org/10.1016/j.jpowsour.2007.06.050.
[60] W. Li, A. Dolocan, P. Oh, H. Celio, S. Park, J. Cho, A. Manthiram, Dynamic behaviour of interphases and its implication on high-energy-density cathode materials in lithium-ion batteries, Nat. Commun. 8 (1) (2017) 1–10, https://doi.org/10.1038/ncomms14589.
[61] M. He, R. Guo, G.M. Hobold, H. Gao, B.M. Gallant, The intrinsic behavior of lithium fluoride in solid electrolyte interphases on lithium, Proc. Natl. Acad. Sci. 117 (1) (2020) 73–79, https://doi.org/10.1073/pnas.1911017116.